Also of significance is the wide range in values that can be attained for a given structural parameter. There has always been a continuing interest in understanding the properties of crystalline polymers in terms of structure. From the present discussion a strategy can be developed where by control of molecular weight and crystallization conditions a specific variable can be isolated[5,6] and its influence on a given property assessed. This procedure has been successfully demonstrated for certain mechanical[64,65] and spectral properties[66] and should be applicable to virtually all properties of crystalline polymers.

(64) Popli, R.; Glotin, M.; Mandelkern, L.; Benson, R. S. *J. Polym. Sci., Polym. Phys. Ed.* **1984**, *22*, 407.

(65) Popli, R.; Mandelkern, L. *J. Polym. Sci., Part B: Polym. Phys.* **1987**, *25*, 441.

(66) Axelson, D. E.; Mandelkern, L.; Popli, R.; Mathieu, P. M. S. *J. Polym. Sci., Polym. Phys. Ed.* **1983**, *21*, 2319.

Valence-Bond Concepts in Transition Metals: Metal Hydride Diatomic Cations

GILLES OHANESSIAN[†] and WILLIAM A. GODDARD III*

Materials Simulation Center of Beckman Institute and Arthur Amos Noyes Laboratory of Chemical Physics,[‡] California Institute of Technology, Pasadena, California 91125

Introduction

Despite the recent advances in understanding bonds between transition metals (TM) and non-metals,[1–7] there remain considerable uncertainties in both the concepts and the thermodynamics of organometallic complexes, severely limiting the understanding of mechanisms for various chemical transformations.[3] In order to provide the flavor of some of the evolving concepts, we will focus here on MH^+ and examine the variations in bond orbitals, bond energies, and other quantities (from both experiment[4] and theory[5]) for the three rows of TM (Sc^+–Cu^+, Y^+–Ag^+, La^+, Hf^+–Au^+) plus the group 2 and group 12 systems. These trends also apply to other bonds to TM, in particular to metal–alkyl[8] and metal–silyl bonds, and should be helpful in estimating and understanding the trends in other TM compounds as well.

The GVB Picture. Typical MH^+ bonds derived from generalized valence bond (GVB) calculations[5] are shown in Figure 1 for FeH^+, RuH^+, and OsH^+. Here we see that the bond pair involves one electron in the hydrogen 1s orbital and one in an sd hybrid on the metal. Thus the bond is covalent (M^+H, not $M^{2+}H^-$). Although the H-centered orbital (right orbitals in Figure

1) remains nearly the same for all cases, there are systematic changes in the hybridization of the TM orbital

(1) (a) Halpern, J. *Acc. Chem. Res.* **1982**, *15*, 238; *Bull. Chem. Soc. Jpn.* **1988**, *61*, 13. (b) Pearson, R. G. *Chem. Rev.* **1985**, *85*, 41. (c) Bryndza, H. E.; Fong, L. K.; Paciello, R. A.; Tam, W.; Bercaw, J. E. *J. Am. Chem. Soc.* **1987**, *109*, 1444. (d) The 1988 issue number 16/17 of *Polyhedron* was fully devoted to organometallic thermochemistry and the energetics of metal–ligand interactions and contains numerous good reviews on this topic. (e) Labinger, J.; Bercaw, J. E. *Organometallics* **1988**, *7*, 926. (f) Mayer, J. M. *Inorg. Chem.* **1988**, *27*, 3899. (g) Martinho-Simoes, J. A.; Beauchamp, J. L. *Chem. Rev.*, submitted for publication.

(2) (a) Goddard, W. A., III. *Science* **1985**, *227*, 917. (b) Rappé, A. K.; Goddard, W. A., III. *J. Am. Chem. Soc.* **1982**, *104*, 448, 3287. (c) Steigerwald, M. L.; Goddard, W. A., III. *Ibid.* **1984**, *106*, 308; **1985**, *107*, 5027. (d) Low, J. J.; Goddard, W. A., III. *Ibid.* **1986**, *108*, 6115. (e) Smith, D. C.; Goddard, W. A., III. *Ibid.* **1987**, *109*, 5580. (f) Carter, E. A.; Goddard, W. A., III. *Organometallics* **1988**, *7*, 675. (g) Anslyn, E. A.; Goddard, W. A., III. *Ibid.* **1988**, *7*, 98; **1989**, *8*, 1550. (h) Allison, J. N.; Goddard, W. A., III. *Chem. Phys.* **1983**, *81*, 263. (i) Steigerwald, J. L.; Goddard, W. A., III, unpublished. See: Steigerwald, M. L. Ph.D. Thesis, California Institute of Technology, 1983 (unpublished).

(3) (a) Connor, J. A. *Top. Curr. Chem.* **1977**, *71*, 71. (b) Reference 1a. (c) Halpern, J. *Inorg. Chim. Acta* **1985**, *100*, 41. (d) Stoutland, P. O.; Bergman, R. G.; Nolan, S. P.; Hoff, C. D. *Polyhedron* **1988**, *7*, 1429.

(4) (a) Armentrout, P. B.; Beauchamp, J. L. *Acc. Chem. Res.* **1989**, *22*, 315 and references therein. (b) Armentrout, P. B.; Georgiadis, R. *Polyhedron* **1988**, *7*, 1573. (c) Elkind, J. L.; Armentrout, P. B. *J. Phys. Chem.* **1987**, *91*, 2037. (d) Beauchamp, J. L. In *High Energy Processes in Organometallic Chemistry*; Suslick, K. E., Ed.; ACS Symposium Series 333; American Chemical Society: Washington, DC, 1987; Chapter 2.

(5) (a) Schilling, J. B.; Goddard, W. A., III; Beauchamp, J. L. *J. Am. Chem. Soc.* **1986**, *108*, 582. (b) Schilling, J. B.; Goddard, W. A., III; Beauchamp, J. L. *J. Phys. Chem.* **1987**, *91*, 5616. (c) Schilling, J. B.; Goddard, W. A., III; Beauchamp, J. L. *J. Am. Chem. Soc.* **1987**, *109*, 5565. (d) Ohanessian, G.; Brusich, M. J.; Goddard, W. A. III. Theoretical Study of Transition Metal Hydrides: V. HfH^+, BaH^+, and LaH^+. *J. Chem. Phys.*, in press.

(6) (a) Harrison, J. F. *J. Phys. Chem.* **1986**, *90*, 3313. (b) Bauschlicher, C. W.; Walch, S. P.; Langhoff, S. R. In *Quantum Chemistry: The Challenge of Transition Metals and Coordination Chemistry*; Veillard, A., Ed.; D. Reidel Publishing Company: Boston, 1986. (c) Ziegler, T.; Tschinke, V.; Ursenbach, C. *J. Am. Chem. Soc.* **1987**, *109*, 1351, 4825.

(7) (a) Harrison, J. F.; Alvarado-Swaisgood, E. *J. Phys. Chem.* **1988**, *92*, 2757. (b) Pettersson, L. G. M.; Bauschlicher, C. W.; Langhoff, S. R.; Partridge, H. *J. Chem. Phys.* **1987**, *87*, 481.

(8) (a) Schilling, J. B.; Goddard, W. A., III; Beauchamp, J. L. *J. Am. Chem. Soc.* **1987**, *109*, 5573. (b) Bauschlicher, C. W.; Langhoff, S. R.; Partridge, H.; Barnes, L. A. *J. Chem. Phys.* **1989**, *91*, 2399.

Table I
Calculated Ground-State Symmetries, Configurations, and Spectroscopic Properties of Metal Hydride Cations[a]

CaH+	ScH+	TiH+	VH+	CrH+	MnH+	FeH+	CoH+	NiH+	CuH+	ZnH+
$^1\Sigma^+(\sigma^0\pi^0\delta^0)$	$^2\Delta(\sigma^0\pi^0\delta^1)$	$^3\Phi(\sigma^0\pi^1\delta^1)$	$^4\Delta(\sigma^0\pi^2\delta^1)$	$^5\Sigma^+(\sigma^0\pi^2\delta^2)$	$^6\Sigma^+(\sigma^1\pi^2\delta^2)$	$^5\Delta(\sigma^1\pi^2\delta^3)$	$^4\Phi(\sigma^1\pi^3\delta^3)$	$^3\Delta(\sigma^1\pi^4\delta^3)$	$^2\Sigma^+(\sigma^1\pi^4\delta^3)$	$^1\Sigma^+(\sigma^2\pi^4\delta^4)$
1.940 Å	1.810 Å	1.730 Å	1.662 Å	1.602 Å	1.702 Å	1.653 Å	1.606 Å	1.561 Å	1.513 Å	1.545 Å
1467 cm⁻¹	1631 cm⁻¹	1696 cm⁻¹	1749 cm⁻¹	1818 cm⁻¹	1570 cm⁻¹	1657 cm⁻¹	1631 cm⁻¹	1728 cm⁻¹	1793 cm⁻¹	1868 cm⁻¹
44.7 kcal	55.2 kcal	54.0 kcal	43.6 kcal	24.3 kcal	39.6 kcal	47.0 kcal	43.6 kcal	35.7 kcal	20.9 kcal	52.4 kcal

SrH+	YH+	ZrH+	NbH+	MoH+	TcH+	RuH+	RhH+	PdH+	AgH+	CdH+
$^1\Sigma^+(\sigma^0\pi^0\delta^0)$	$^2\Sigma^+(\sigma^1\pi^0\delta^0)$	$^3\Phi(\sigma^0\pi^1\delta^1)$	$^4\Delta(\sigma^0\pi^2\delta^1)$	$^5\Sigma^+(\sigma^0\pi^2\delta^2)$	$^6\Sigma^+(\sigma^1\pi^2\delta^2)$	$^3\Sigma^-(\sigma^0\pi^4\delta^2)$[b]	$^2\Delta(\sigma^0\pi^4\delta^3)$	$^1\Sigma^+(\sigma^0\pi^4\delta^4)$	$^2\Sigma^+(\sigma^1\pi^4\delta^4)$	$^1\Sigma^+(\sigma^2\pi^4\delta^4)$
2.079 Å	1.892 Å	1.857 Å	1.764 Å	1.708 Å	1.719 Å	1.581 Å	1.539 Å	1.512 Å	2.428 Å	1.709 Å
1346 cm⁻¹	1639 cm⁻¹	1658 cm⁻¹	1805 cm⁻¹	1826 cm⁻¹	1737 cm⁻¹	1986 cm⁻¹	2125 cm⁻¹	2127 cm⁻¹	372 cm⁻¹	1696 cm⁻¹
44.1 kcal	57.8 kcal	54.6 kcal	48.7 kcal	31.2 kcal	46.3 kcal	31.7 kcal	34.8 kcal	40.6 kcal	2.1 kcal	42.0 kcal

BaH+	LaH+	HfH+	TaH+	WH+	ReH+	OsH+	IrH+	PtH+	AuH+	HgH+
$^1\Sigma^+(\sigma^0\pi^0\delta^0)$	$^2\Delta(\sigma^0\pi^0\delta^1)$	$^3\Delta(\sigma^1\pi^0\delta^1)$	$^4\Sigma^-(\sigma^1\pi^2\delta^0)$[b]	$^5\Pi(\sigma^1\pi^1\delta^2)$	$^6\Sigma^+(\sigma^1\pi^2\delta^2)$	$^5\Pi(\sigma^1\pi^3\delta^2)$	$^4\Sigma^-(\sigma^1\pi^4\delta^2)$[b]	$^1\Sigma^+(\sigma^0\pi^4\delta^4)$	$^2\Sigma^+(\sigma^1\pi^4\delta^4)$	$^1\Sigma^+(\sigma^2\pi^4\delta^4)$
2.202 Å	2.093 Å	1.786 Å	1.741 Å	1.701 Å	1.659 Å	1.605 Å	1.560 Å	1.519 Å	1.539 Å	1.627 Å
1408 cm⁻¹	1513 cm⁻¹	1979 cm⁻¹	2006 cm⁻¹	2065 cm⁻¹	2065 cm⁻¹	2244 cm⁻¹	2372 cm⁻¹	2399 cm⁻¹	2273 cm⁻¹	1888 cm⁻¹
50.9 kcal	60.4 kcal	54.9 kcal	54.0 kcal	49.9 kcal	44.5 kcal	56.2 kcal	65.8 kcal	62.9 kcal	33.4 kcal	48.6 kcal

[a] The quantities in parentheses $(\sigma^i\pi^j\delta^k)$ indicate the numbers of nonbonding valence electrons in various orbitals (i in d_σ, j distributed among d_{π_x} and d_{π_y}, and k distributed among $d_{\delta_{xy}}$ and $d_{\delta_{x^2-y^2}}$). In each case the highest spin allowed by these configurations is the ground state. The equilibrium bond distance (Å), vibrational frequency (cm⁻¹), and bond energy (D_0 in kcal/mol) are also indicated. [b] The following molecules have a second important configuration: $RuH^+(\sigma^0\pi^2\delta^4)$, $TaH^+(\sigma^1\pi^0\delta^2)$, and $IrH^+(\sigma^1\pi^2\delta^4)$.

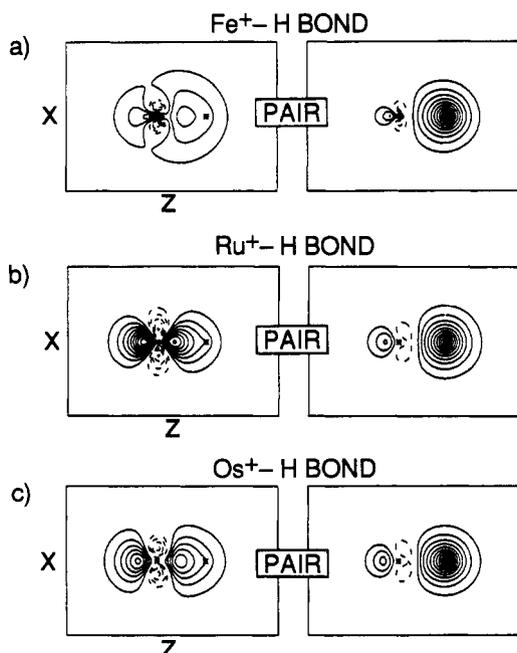a)

Fe+– H BOND

b)

Ru+– H BOND

c)

Os+– H BOND

Figure 1. GVB bonding orbitals at R_e for (a) FeH+, (b) RuH+, and (c) OsH+. Solid lines indicate positive amplitudes, while dotted lines indicate negative amplitudes. The spacing between contours is 0.05 au. The contours are plotted in the xz plane with the M+-H bond along the z axis. The plot limits are –3.0 to +4.0 Å for the z axis and –2.5 to +2.5 Å for the x axis.

that arise directly from the properties of M+ ions. Thus the electronic configuration (occupied orbitals) can be understood in terms of the orbitals present on M+ in its ground state or lowest excited state. The condition of making a covalent bond to H eliminates most possible orbital occupations leading, in all cases, to the low-lying states of MH+.

The ground state of M+ is either d^n or s^1d^{n-1} (see Figure 2), where n is the number of valence electrons (there are two exceptions: Y+ and Hf+, with s^2d^{n-2} ground configurations). We classify these orbitals by their diatomic symmetry (z is the molecular axis): δ for d_{xy} and $d_{x^2-y^2}$, π for d_{xz} and d_{yz}, and σ for d_{z^2} and s. For instance, starting with Fe+ in the s^1d^6 configuration, the H bonds to the 4s orbital, leaving a nonbonding configuration based on d^6: $\sigma^2\pi^2\delta^2$, $\sigma^1\pi^3\delta^2$, or $\sigma^1\pi^2\delta^3$.
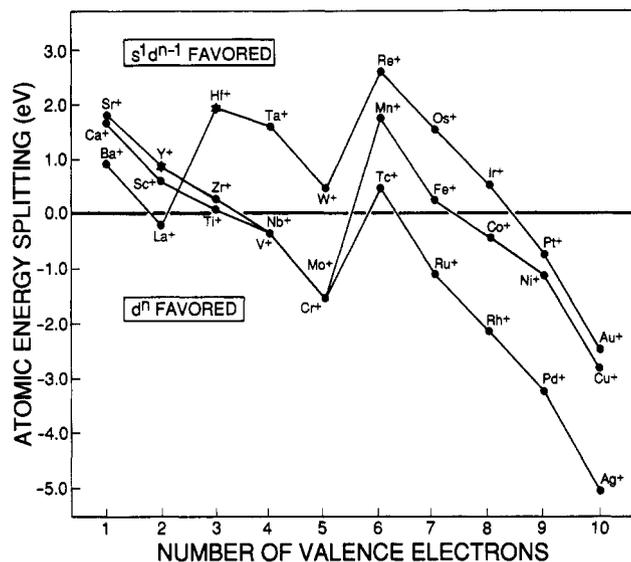
Figure 2. Energy difference between the lowest metal cation electronic states arising from d^n and s^1d^{n-1} configurations. $\Delta E = E_{d^n} - E_{s^1d^{n-1}}$. In each case the experimental states have been averaged over J to obtain LS state energies. The stars on Y+ and Hf+ indicate that s^2d^{n-2} is the ground configuration in these cases.

Orbital Configurations of MH+

The predicted ground-state symmetries and configurations for MH+ are given in Table I. These configurations (and those of the low excited states) can be predicted by using *the GVB model*:

(1) Start with the ground configuration of M+ (generally either d^n or s^1d^{n-1}), where it is understood that the spin is the highest possible (Hund's rule).

(2) While retaining the same number of unpaired orbitals, distribute the electrons so as to reserve a singly occupied σ orbital for binding to the H while minimizing the number of other σ electrons (which would have unfavorable interactions with the former). This means that early TM hydrides generally avoid having nonbonding σ electrons, while late metals prefer having one to help relieve repulsions in other (π and δ) nonbonding orbitals.

(3) If there is a choice in the distribution of π and δ electrons, use the one with the lowest total electron repulsion in the atom.

388 *Acc. Chem. Res., Vol. 23, No. 11, 1990*

Ohanessian and Goddard

(4) In some cases there is a conflict among the above prescriptions in that the distribution of nonbonding electrons minimizing the total electron repulsion corresponds to an excited configuration of the metal cation. If the promotion energy required to reach that configuration is low enough to offset the increase of electron repulsion, the ground state of MH^+ is formed with the excited configuration of M^+.

As an example of step 2, bonding H to the 4s orbital of Sc^+ leads to a nonbonding singly occupied d orbital that can be σ, π, or δ. The σ is worst because it must be orthogonal to the bond pair (Pauli principle), while δ is best because it has the smallest electrostatic interaction with the bonding electrons. For ScH^+ this leads to the $^2\Delta(\delta^1)$ ground state, where the δ^1 in parentheses indicates the occupation of *nonbonding* orbitals.

As an example of step 3, for VH^+ we bond the H to the σ orbital of either the $\sigma^1\pi^2\delta^1$ or $\sigma^1\pi^1\delta^2$ configuration of V^+. The δ^2 configuration has a high electron repulsion energy (with two electrons in the xy plane) so that $^4\Delta(\pi^2\delta^1)$ is the ground state.

For $Ti^+(s^1d^2)$ this analysis leads to the $^3\Phi(\pi^1\delta^1)$ ground state, while for $Cr^+(d^5)$ it leads to the $^5\Sigma^+(\pi^2\delta^2)$ ground state. Similarly for $Mn^+(s^1d^5)$, we obtain a $^6\Sigma^+(\sigma^1\pi^2\delta^2)$ ground state, where a nonbonding σ orbital must now be singly occupied. For $Fe^+(s^1d^6)$ we obtain $^5\Delta(\sigma^1\pi^2\delta^3)$, where it is best to have the extra electron in δ (farthest away from the bond).

For Co^+, Ni^+, and Cu^+, the best bonds are obtained by using the s^1d^{n-1} *excited* states. This occurs because (1) the d orbitals are too small for good bonding and (2) the s^1d^{n-1} states are low-lying. The result is $^4\Phi(\sigma^1\pi^3\delta^3)$ for CoH^+, $^3\Delta(\sigma^1\pi^4\delta^3)$ for NiH^+, and $^2\Sigma^+(\sigma^1\pi^4\delta^4)$ for CuH^+.

The second transition row differs from the first primarily for the late half, where stabilization of d^n is so strong that RuH^+, RhH^+, and PdH^+ are all based on d^n rather than s^1d^{n-1}, leading to $^3\Sigma^-(\pi^4\delta^2)$, $^2\Delta(\pi^4\delta^3)$, and $^1\Sigma^+(\pi^4\delta^4)$, respectively. The other difference is for YH^+, which is $^2\Sigma^+(\sigma^1)$ because Y^+ has an s^2 ground state.

In the third row, the dominant feature is the extra stabilization of s^1d^{n-1} over d^n, associated with the much larger relativistic effects after the lanthanides. In addition, the size and directionality of the 5d orbital allows good overlap with the H (better than 6s) so that σ nonbonding orbitals have large s character. Indeed, all hydrides from HfH^+ to HgH^+ (except for PtH^+) have one or two electrons in the nonbonding σ orbital (see Table I). Thus HfH^+, TaH^+, and WH^+ have the nonbonding σ orbital singly occupied, in contradistinction with the first- and second-row congeners.

Nature of the Metal–Hydrogen Bond

Hybridization. All calculations show that the M^+–H bond pair involves one electron in a metal valence orbital that is a mixture of valence s and d character with little valence p. However, the relative amounts of s–d hybridization vary considerably among the rows, as indicated in Figure 3. The trends are as follows:

(a) In the first row the 4s orbital is much larger than 3d (Figure 4), making the 4s more available for the bond to H and therefore dominant. The hybridization is about 45% s for ScH^+ through CrH^+ and about 75% s for MnH^+ through CuH^+. The reason for this change is the presence of a σ nonbonding electron starting with
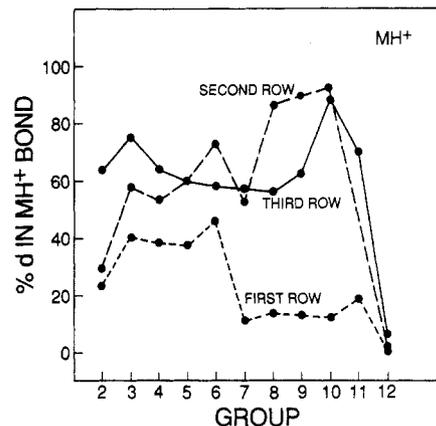

Figure 3. Percentages of d orbital character in the GVB metal bonding orbital centered on the metal; based on Mulliken populations where the total on the atom is normalized. (AgH^+ is omitted because no covalent bond is formed.)
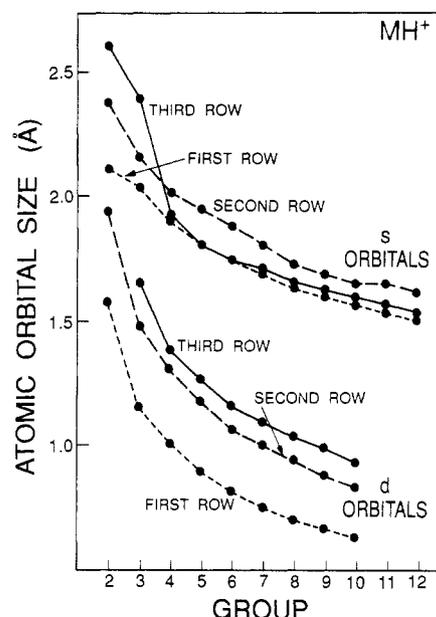
Figure 4. Sizes of metal valence s and d atomic orbitals. The size is defined as $(\langle\phi|r^2|\phi\rangle)^{1/2}$ from Hartree–Fock calculations.

MnH^+. The σ nonbonding orbital must be orthogonal to the bond pair, and this is done at much lower energy cost by using the d_{z^2} (which does not overlap the H well), thereby enhancing the s contribution to the bond. Since Zn^+ has only the $^2S(s^1d^{10})$ state available, there is no possibility for d bonding, leading to ZnH^+ with 90% s character (see Figure 3) and a longer bond. The same reasoning applies to the other group 12 hydrides, CdH^+ and HgH^+.

(b) In the second row, the 5s and 4d orbitals are more similar in size (Figure 4), leading to much larger d character in the bond orbitals. There is a gradual increase of d character (Figure 3) from YH^+ (57%) to PdH^+ (93%) because the d^n configurations of M^+ are particularly stable in late second row metals (see Figure 2). However, there is low d contribution to the TcH^+ bond due to the special stability of the high-spin nonbonding d^5 configuration, which is preserved only if the bond is to the s orbital (the same effect was operative in MnH^+ but did not lead to a discontinuity in the first row because all late-metal hydrides have high s character).

Figure 5. Charge transfer in the M^+–H bonds; the total Mulliken population on the H from GVB wave functions.

(c) The trend is smoother again in the third row, where 60% d character is maintained from HfH^+ to IrH^+. (Ignoring exchange and promotion effects, 60%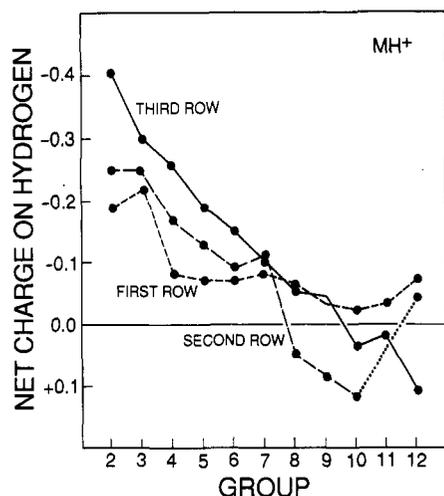 d character leads to the maximum bond stabilization.[2c,d,i]) An increase occurs for PtH^+ and AuH^+ because the ground configuration of M^+ is d^n in these cases.

Charge Transfer. The GVB calculations show a small amount of charge transfer between M^+ and H in almost all cases. The result is a fairly covalent bond. This is at variance with the traditional oxidation-state formalism, which would consider the charge distribution as $M^{2+}H^-$. The net charge transfer in the hydride bonds is depicted in Figure 5. Within each row, the TMs get more electronegative with increasing atomic number (ranging from $Q_H = -0.28$ in group 2 to $Q_H = +0.03$ in group 10 and $Q_H \approx 0$ in groups 11 and 12). This is analogous to the trend in main-group elements and relates to the increasing effective nuclear charge seen by the valence electrons.

The trends within columns are less clear-cut:

(a) Early-metal cations (groups 2–6) get more *electropositive* in going down a column (just as for main-group elements).

(b) Group 7 cations (Mn^+, Tc^+, and Re^+) transfer about the same amount of charge to H.

(c) Groups 8–10 have the second-row metal much more electronegative than either the first- or third-row metal.

(d) Groups 11 and 12 cations become more *electronegative* in going down the periodic table (opposite to the tendency for main-group elements).

However, the deviations in charges within a column tend to be less than 0.05.

Bond Lengths. The trends in bond distances for MH^+ are dominated by the sizes of the metal atomic orbitals (see Figure 4). Orbital sizes scale as n^2/Z_{eff}, where n is the principal quantum number and Z_{eff} is the effective nuclear charge felt by the electron. Thus the main difference between the sizes of valence orbitals is that the valence s orbital has a value of n one unit larger than the valence d orbital (e.g., 4s versus 3d), making s significantly more diffuse than d. This is particularly true for first-row metals in which the 3d shell has no underlying core d electron and is therefore unusually contracted (no Pauli orthogonality). As a result, for

first-row metals the s orbitals are more readily available for bonding than the d. This difference tends to fade going down the periodic table, so that d orbitals become more involved in the bond. In the third row, the lanthanide contraction strongly perturbs this effect.

A second trend is that the s and d orbitals both contract to the right in each row. The difference in principal quantum number and the differential shielding effects make this a stronger effect for d than for s orbitals. In particular, the lanthanide contraction leads to a huge tightening of s orbitals between La^+ and Hf^+ (see Figure 4).

The bond length is determined by the interplay of three different metal orbitals: the valence s and d_σ (of which the bonding orbital is a blend) and the outer *core* p orbital, which sets up a repulsive wall (Pauli orthogonality) against the approach of H. Since the bonding orbital undergoes significant changes in character (hybridization) across rows and down columns of the periodic table, we did not expect the bond length to correlate with the size of *either* the s or d_σ metal valence orbital. However, the MH^+ bond distance (see Table I) correlates well with the size of the valence s orbital (much better than it does with other metal orbitals). In particular, the bond lengths for M = Mn through Cu and M = W through Au are within 0.05 Å of the size of the valence s orbital. The second-row TMs and early TMs have bonds shorter by 0.2 Å, due to the strong role of the d orbitals.

Bond Energies

Having examined the factors dominating the *nature* and *length* of the bonds, we now consider *bond strength*. The bond energies of the metal hydrides (Figures 6 and 7) show a number of complicated patterns. The major factors here are (i) the change in atomic exchange energy and (ii) the promotion energy to obtain an atomic configuration suitable for bonding. In this section we will first analyze these factors and then discuss the trends in bond energies.

Orbital Configurations of M^+. To analyze the trends in bond energies it is important to understand the origin of the fluctuations in the atomic configurations in Figure 2. As the nd and $(n + 1)s$ atomic orbitals are progressively filled, the lowest lying configurations of the TM ions follow simple building rules:

(i) As many orbitals as possible are kept singly occupied in order to minimize the total Coulombic repulsion.

(ii) The electrons in singly occupied orbitals are coupled high-spin to maximize exchange stabilization (Hund's rule).

Therefore, the ground configurations of the cations are generally either d^n or $s^1 d^{n-1}$.

The leading trend is a special stability of d^n as the d shell approaches being half-filled (d^5) or nearly completely filled (d^{10}). This arises from the larger exchange stabilization between two electrons in d orbitals ($-K_{dd'}$) than between s and d electrons ($-K_{sd}$). The first two transition rows yield very similar trends except that the late members of the second row have greater stability for d^n. This arises because the self-shielding between the d orbitals of the second row is smaller (since the d orbitals are larger).

An additional effect—the lanthanide contraction—occurs between La and Hf. The increase of nuclear
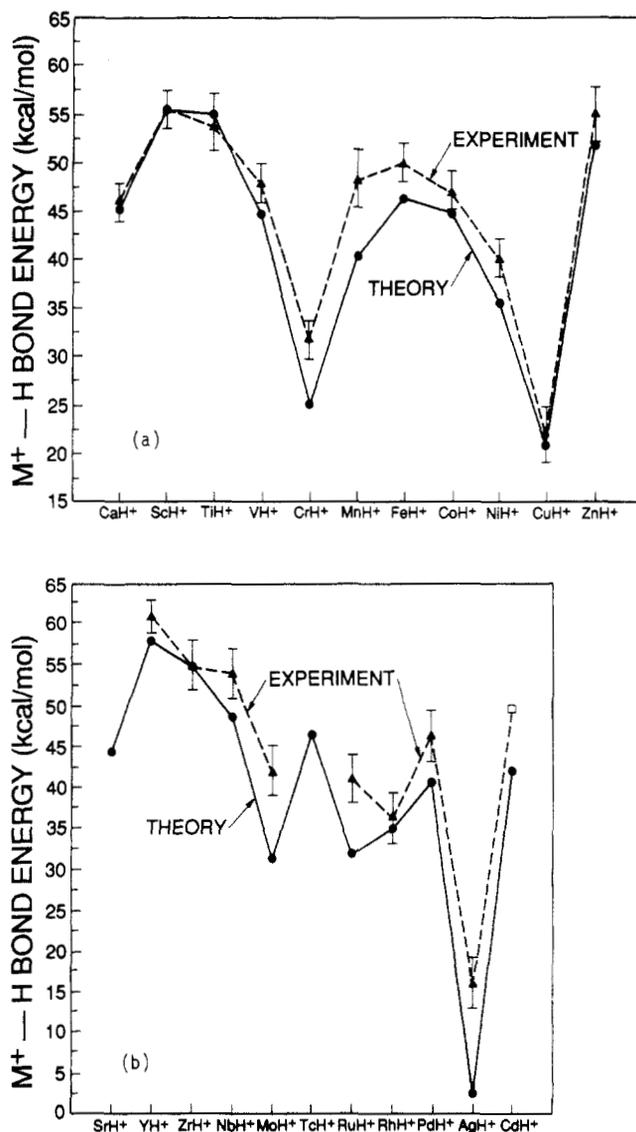
Figure 6. Calculated and experimental bond energies in TM hydride cations (experimental values from ref 4a): (a) first row; (b) second row.

charge by 14 units causes a strong tightening of the valence s orbitals. This arises from two effects:

(a) The additional nuclear charge is only partially screened by the filled 4f orbitals. This effect is much stronger for s than for d orbitals, since d orbitals go to zero at the nucleus.

(b) Relativistic effects decrease the kinetic energy of the inner s orbitals, allowing the orbitals to contract. This results in differential stabilization and contraction of all s orbitals (thereby increasing kinetic energy) as is clear in Figures 2 and 4, respectively. The contracted s orbitals provide additional shielding to the d orbitals, whose contraction (and therefore stabilization) is much more limited. The overall effect is to greatly stabilize the s-occupied configurations. Thus the ground state of W^+ is s^1d^4 rather than d^5 (as are Cr^+ and Mo^+), and the ground configuration of Hf^+ is s^2d^1 rather than s^1d^2 (as are Ti^+ and Zr^+). In turn, the nature of the M^+ ground state (d^n or s^1d^{n-1}) has a strong influence on the character and bond energy of the ground state of MH^+, leading to characteristic differences for the post-lanthanides.

Nonbonding Electrons Come into Play: Exchange Energy Loss. So far we have focused on in-
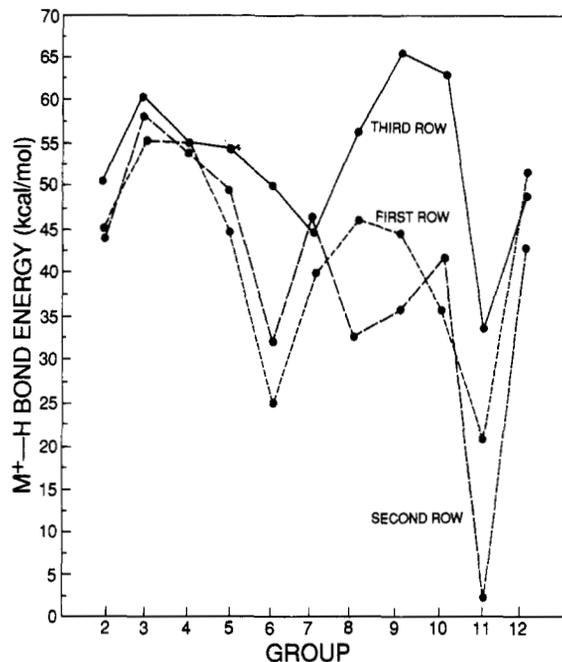
Figure 7. Calculated bond energies for all three rows of TM hydride cations.

Table II
Exchange Energies (kcal/mol) for Mn^+, Tc^+, and Re^{+a}

metal	K_{sd}	$K_{dd'}$
Mn^+	4.8	19.8
Tc^+	8.3	15.3
Re^+	11.9	14.1

[a] From atomic Hartree–Fock wave functions of the $^6S(s^1d^5)$ states. The d–d energies are averaged over d orbitals.

teractions involving the *bonding* electrons. The *nonbonding* electrons also play an important role in determining the bond energies because they control the amount of metal exchange energy lost upon bonding. Thus, the relative energies of the lowest metal states are largely determined by the relative amounts of exchange energy. Consequently, when the electron in a singly occupied orbital on the metal is spin-paired with the electron in the H orbital, it can no longer be coupled high-spin with the other metal electrons, leading to a loss in the atomic exchange stabilization.[9,10] To estimate this change, consider that the bond pair has the spin function $(\alpha\beta - \beta\alpha)$ so that the metal orbital is half α and half β. As a result, half of the exchange energy between the metal bonding orbital and the nonbonding metal orbitals may be lost.[9,10,11a] Thus, for group 3 hydrides (one nonbonding electron) there is a loss of $K/2$ upon bond formation, a loss that increases uniformly to a total of $5K/2$ for group 7 hydrides (five unpaired nonbonding electrons). Beginning with group 8, the presence of both α and β nonbonding orbitals leads to a decreased exchange loss that drops to zero in group 12 hydrides. The consequence is a maximum exchange loss of bond energy near the middle of each row.

(9) Goddard, W. A., III; Harding, L. B. *Annu. Rev. Phys. Chem.* **1978**, *29*, 363.

(10) Carter, E. A.; Goddard, W. A., III. *J. Phys. Chem.* **1988**, *92*, 5679.

(11) (a) This description is oversimplified; if the exchange loss is too large, the bond pair may have some triplet character ($\alpha\beta + \beta\alpha$), leading to a weaker bond but a larger exchange energy. (b) This description is oversimplified. The actual state on the metal is a mixture of d^n and s^1d^{n-1}, so that the lowering of the bond energy is a fraction of the atomic-state splitting.

In order to quantify this loss, we have to consider the character (mainly s or d) of the metal bonding orbital. This is because the $K_{dd'}$ exchange integrals are significantly larger than those of the K_{sd} type (see Table II), but the difference decreases in going down the columns.

Quantitative Estimate of Promotion Energies and Exchange Losses. Given the dominant character of the metal bonding orbital, we can now evaluate the effects of both promotion energy and exchange loss. For the first-row metals, the bonding involves primarily the 4s metal orbital. Thus, metal ions having a d^n ground state (V^+, Cr^+, Co^+, Ni^+, and Cu^+) must be promoted to the lowest lying s^1d^{n-1}-type excited state to be prepared for bonding. Since the dissociation limit involves ground-state atoms, the bond energy is reduced accordingly.[11b] For the second row, such promotion effects are involved in Y^+ and Ag^+, and for the third row, they are required for Au^+.

As discussed in the previous section, the maximum exchange loss is for group 7 metals. The magnitude of the exchange integrals is fairly constant across the row, leading to a monotonic increase from Ca^+ to Mn^+ and decrease from Mn^+ to Zn^+.

Bond Dissociation Energies. The general patterns of bond energies across each row are similar, as shown in Figures 6 and 7, and illustrate the interplay of factors described in previous sections. The major features are as follows:

(1) The combined effects of metal promotion energy and exchange loss (vide supra) lead to low bond energies near the middle and end of each row.

(2) The M^+–H bond strengths are similar for first- and second-row metals but significantly stronger in the third row. The origin of this is now discussed.

For the second and third rows the promotion and exchange energies behave similarly to those for the first row, but with some important variations. Consider, for example, group 6 metal hydrides. The bond in CrH^+ is particularly weak because of the promotion energy (d^5 to s^1d^4) required for Cr^+ to make an s-like bond to H. For the second row, d bonding is more favorable, and thus the ^6S of the $Mo^+(d^5)$ ground state is adequate for the bond in MoH^+. However, the exchange loss for MoH^+ is $2K_{dd'}$ (instead of $2K_{sd}$ as in CrH^+), and therefore the Mo^+–H bond is still weak. For the third row, d bonding is quite favorable. Since the ground state of W^+ is now $^6D(s^1d^4)$, the bond can mix s and d components without promotion energy. Here the higher s character of the metal bonding orbital (compared with MoH^+) helps minimize the exchange loss, making the W^+–H bond the strongest in group 6. These same factors (maximum exchange loss) make ReH^+ (group 7) the weakest bond in the third series (except for AuH^+), whereas the group 6 case is the weakest in the first two rows.

The pattern in bond energies for the late second row, MoH^+ through PdH^+ (Figure 7), is significantly different from those for the corresponding first- and third-row metals. Tc^+ with a $^7S(s^1d^5)$ ground state could use either an s or a d orbital to bind to H, but it prefers s character (to retain the high-spin d^5 shell), so that the exchange loss in TcH^+ involves K_{sd} terms. In contrast, Mo^+, Ru^+, Rh^+, and Pd^+ all have ground d^n configurations and large d^n to s^1d^{n-1} splittings, leading to d bonding and much larger $K_{dd'}$ exchange losses. As a

result, these four bonds are weaker than the bond in TcH^+.

In noble metal hydrides, the $^1S(d^{10})$ ground state of M^+ cannot form a bond with the H since there is no singly occupied metal orbital. The excited $^3D(s^1d^9)$ state has a singly occupied orbital for bond formation but requires a large promotion energy (see Figure 2). This promotion energy to the ^3D state of M^+ is so high (2.4 eV for Au^+, 2.8 eV for Cu^+, and 5.0 eV for Ag^+) that the full wave function (including electron correlation) contains a large amount of local metal d^{10} character, even though this is at the expense of removing one of the two bonding electrons. As a result, the bond energies are drastically reduced (see Figure 7). In fact, the promotion energy for Ag^+ is so high that a covalent bond cannot be formed at all, resulting in a loose ion–dipole Ag^+–H complex with a bond strength of only 2.1 kcal/mol.

Summarizing, the strong variations of bond energies shown in Figures 6 and 7 are dominated by fluctuations in the promotion and exchange energies of M^+ upon binding to H. Excluding such effects leads to intrinsic bond strengths[5] that are much more constant across each row.

The 5d orbitals of third-row metals are larger than the 4d orbitals in the second, leading to better overlap. The 6s orbitals in the third row are *tighter* than the 5s orbitals in the second row, and this again leads to larger overlap. The overall effect is a significant increase in bonding interaction, leading to significantly larger bond energies. The bond strengths in the first and second rows are similar because the larger d character in second-row hydride bonds (which would lead to greater strength) is largely cancelled by the smaller size of the bonding orbital (5d for second row and 4s for first row; see Figure 4).

Summary

The GVB view of bonding in MH^+ can be summarized as follows:

(a) Start with the ground configuration of M^+.

(b) Spin-pair a singly occupied σ orbital of M^+ to the H 1s orbital to form the bond.

(c) If more than one type of orbital is available for the bond (e.g., 6s versus 5d), choose the one with the best overlap.

(d) For degenerate states of M^+, choose the occupations of π and δ orbitals with the lowest electron repulsion.

(e) Examine the loss in exchange energy due to pairing of the σ orbital to H. If the loss is large, consider low-lying excited states, M^{+*}, that might have a stronger bond or lower exchange loss. If these factors exceed the promotion energy to the excited state, the bond is formed from M^{+*}.

We have found these principles to be generally valuable for predicting the ground states of other transition-metal complexes[2] and of reaction intermediates. Thus, one (a) considers the ground states of fragments A and B, (b) orients them to get the best bonds, and (c) considers loss in intrafragment exchange and possible promotion to excited configurations.

Our inspiration in using valence bond concepts for transition metals derives from Linus Pauling's classic,[12] Nature of the

(12) Pauling, L. *Nature of the Chemical Bond*, 3rd ed.; Cornell University Press: Ithaca, NY, 1960.

Chemical Bond. We hope the ideas here show how VB concepts can provide additional qualitative and quantitative understanding of transition-metal systems. The systematic studies on the first two rows of TM hydrides carried out with Dr. J. B. Schilling (now at Amoco Research Center) and Prof. J. L. Beauchamp[5a–c] (Caltech) led to the concepts that form the basis of this review. The similar studies on the third row TM hydrides with M. J. Brusich[5d] (now at IDA) are combined here with the earlier ones to provide an overview of MH⁺ bonds for all three rows. Some of these concepts go back to the earliest GVB

Model Reactions for Characterizing the Acidity of Solid Catalysts

MICHEL R. GUISNET

URA CNRS DO 350, Catalyse en Chimie Organique, Université de Poitiers, 40, avenue du Recteur Pineau, 86022 Poitiers Cedex, France

Solid acid catalysts are the backbone of major processes of refining and of petrochemistry: cracking, hydrocracking, reforming, isomerization, and disproportionation of aromatics. These catalysts, in the near future, should also play a significant role in the synthesis of functional compounds.[1] The participation of natural acid solids (in particular clays) as catalysts in the formation of petroleum is also well-known.[2]

There exist a large variety of solid acids:[3] natural clay minerals, mounted acids (H_3PO_4 mounted on diatomaceous earth), cation-exchange resins (Nafion), oxides (alumina) and mixtures of oxides (silica–alumina), salts ($MgSO_4$), and zeolites. The acidity of these solids even within a class can be completely different: Some solids can be considered as superacid while others have a very reduced acid strength.

In reactions occurring by acid catalysis, the activity, stability, and selectivity of acid solids are obviously determined to a large extent by their surface acidity (i.e., the number, nature, strength, and density of their acid sites). The acidity required for catalyzing the transformation of reactants into valuable products or into byproducts can be quite different. Indeed, certain reactions demand very strong acid sites while others can be catalyzed by very weak acid sites.[4] The rate of certain bimolecular reactions depends on the space between acid sites probably because their catalysis requires several acid sites.[5–9] However, for skeletal transformations of hydrocarbons, the rate depends essentially on the Brönsted acidity of the catalysts.[4,10] Good correlations have been obtained between the concentration of Brönsted sites and the rate of cumene dealkylation,[11,12] xylene isomerization,[13] toluene[14] and ethylbenzene[15,16] disproportionation, *n*-hexane crack-

ing,[17] etc. Apparently, the Lewis acid sites alone are not active in these reactions. However, it has been shown that Lewis acid sites in the vicinity of protonic sites can increase their strength and consequently their activity.[18] The dependence of catalytic properties on the acid properties of solid catalysts is often more complex for the reactions of functional compounds. The acid sites (Lewis and/or Brönsted) and base sites, which coexist in adjacent positions on the surface of acid catalysts, participate together in most of these reactions[3] (acid–base bifunctional catalysis).

The rate and selectivity of reactions that do not occur by acid catalysis can also be affected by acidity. This has been shown in the case of oxidation of hydrocarbons on transition-metal oxides. Acid–base properties of

(1) Hoelderich, W. F. *Zeolites, Facts, Figures, Future*; Jacobs, P. A., Van Santen, R. A., Eds.; Studies in Surface Science and Catalysis 49; Elsevier: Amsterdam, 1989; pp 69.93.
(2) Tissot, B. P.; Welte, D. H. *Petroleum formation and occurrence*; Springer-Verlag: Berlin, 1978.
(3) Tanabe, K. *Solid Acids and Bases*; Academic Press: New York, 1970.
(4) Guisnet, M. *Catalysis by Acids and Bases*; Imelik, B., et al., Eds.; Studies in Surface Science and Catalysis 20; Elsevier: Amsterdam, 1985; pp 283–297.
(5) Bierenbaum, H. S.; Partridge, R. D.; Weiss, A. H. *Adv. Chem. Ser.* **1973**, *121*, 605–617.
(6) Martin de Armando, M. L.; Gnep, N. S.; Guisnet, M. *J. Chem. Res., Synop.* **1981**, 8–9; *J. Chem. Res., Miniprint* **1981**, 243–255.
(7) Guisnet, M.; Avendano, F.; Bearez, C.; Chevalier, F. *J. Chem. Soc., Chem. Commun.* **1985**, 336–337.
(8) Giannetto, G.; Sansare, S.; Guisnet, M. *J. Chem. Soc., Chem. Commun.* **1986**, 1302–1303.
(9) Jacquinot, E.; Raatz, F.; Macedo, A.; Marcilly, C. *Zeolites as Catalysts, Sorbents and Detergent Builders*; Karge, H. G., Weitkamp, J., Eds.; Studies in Surface Science and Catalysis 46; Elsevier: Amsterdam, 1989; pp 115–125.
(10) Benesi, H. A.; Winquist, B. H. C. *Adv. Catal.* **1978**, *27*, 97–182.
(11) Turkevich, J.; Ono, Y. *Adv. Catal.* **1969**, *20*, 135–152.
(12) Jacobs, P. A.; Leeman, H. E.; Uytterhoeven, J. B. *J. Catal.* **1974**, *33*, 17–30.
(13) Ward, J. W.; Hansford, R. C. *J. Catal.* **1969**, *13*, 154–160.
(14) Aonuma, T.; Sato, M.; Shiba, T. *Shokubai* **1963**, *5*, 274–277.
(15) Karge, H. G.; Ladbeck, J.; Sarbak, Z.; Hatada, K. *Zeolites* **1982**, *2*, 94–102.
(16) Karge, H. G.; Hatada, K.; Zhang, Y.; Fiedorow, R. *Zeolites* **1983**, *3*, 13–21.
(17) Ward, J. W. *J. Catal.* **1968**, *10*, 34–46.
(18) Mirodatos, C.; Barthomeuf, D. *J. Chem. Soc., Chem. Commun.* **1981**, 39–40.

Professor Michel R. Guisnet was born in 1939 in Cambrai, France. He received his B.Sc. and M.Sc. degrees from the University of Lille and his Ph.D. degree from the University of Poitiers. He is the Director of the Laboratory of Catalysis in Organic Chemistry of the University of Poitiers, which is associated with the French National Center of Scientific Research (CNRS). His research has dealt mainly with acid and bifunctional catalysis on zeolites in relation with refining and petrochemistry processes and more recently with fine chemical synthesis.